ChemPubSoc Europe

DOI: 10.1002/chem.201903408

CHEMISTRY A European Journal Communication

Supramolecular Chemistry

A Molecular Approach for Mitigation of Aluminum Pitting based on Films of Zinc(II) and Gallium(III) Metallosurfactants

A. D. K. Isuri Weeraratne, Chathuranga C. Hewa-Rahinduwage, Sunalee Gonawala, Long Luo,* and Cláudio N. Verani*[a]

Abstract: The use of metallosurfactants to prevent pitting corrosion of aluminum surfaces is discussed based on the behavior of the metallosurfactants $[Zn^{II}(L^{N2O2})H_2O]$ (**1**) and $[Ga^{III}(L^{N2O3})]$ (**2**). These species were deposited as multilayer Langmuir–Blodgett films and characterized by IR reflection absorption spectroscopy and UV/Vis spectroscopy. Scanning electron microscopy images, potentiodynamic polarization experiments, and electrochemical impedance spectroscopy were used to assess corrosion mitigation. Both metallosurfactants demonstrate superior anticorrosion activity due to the presence of redox-inactive $3d^{10}$ metal ions that enhance the structural resistance of the ordered molecular films and limit chloride mobility and electron transfer.

Aluminum is a light, malleable, moldable, and nonmagnetic metal that resists atmospheric corrosion, and displays electrical and thermal conductivity. These attributes enable wide use in automotive, aerospace, and naval industries. Although the metal is the third most abundant element in the crust (80 700 ppm), isolation from bauxite has a high environmental cost and generates an estimated 13 tons of CO_2 per ton of Al,[1] along with a toxic solid waste known as red mud. As such, conservation efforts are necessary at all levels and include recycling and corrosion mitigation.

Unlike iron, in which adventitious oxygen and water leads to the formation of $Fe(OH)_3$ and Fe_2O_3,[2–6] the mechanisms of Al corrosion are more complex and less understood. Nonetheless, the action of pitting corrosion leads to pernicious structural failures in car frames, airplane fuselages, and ship hulls, and demands immediate attention. With an electronic configuration given by [Ne] $3s^2\ 3p^1$, the metal has a standard potential of $-1.7\ V_{SHE}$ associated with the loss of the $3s^2$ and $3p^1$ electrons during the process given by $Al_{(s)} \rightleftharpoons Al^{3+} + 3\,e^-$. Pitting is initiated in neutral media by the presence of chloride[7] and other anions[8] that physisorb at the positively charged surface of the Al_2O_3 passivation layer.[2,9] The Cl^- anions penetrate through nanometer-sized cracks or migrate via oxygen vacancies[10–12] reaching the $Al_2O_3\,|\,Al^0$ interface, quickly converting Al^0 into $AlCl_3$, and then the anionic tetrahedral[13] complex $[Al^{III}Cl_4]^-$. This soluble anion reacts with water forming aluminum hydroxide, given by $[Al^{III}Cl_4]^- + 3\,H_2O \rightarrow [Al^{III}(OH)_3] + 3\,H^+ + 4\,Cl^-$. The propagation phase yields localized blisters of acidic pH that eventually erupt and expose the corrosion pit.[14] The corrosion rate decreases over time, but perforation may occur, and chromium-based coatings have been commonly used.[15,16] However, concerns with the environmental impact of hexavalent chromium generated by these coatings impose steep restrictions to their use.[16] In searching for potential alternatives, we hypothesize that the presence of an ordered Langmuir–Blodgett (LB) multilayer of molecular metallosurfactants would act as a hydrophobic barrier that decreases access of water, dissolved chlorides and electrons to the Al_2O_3 layer. In this paper we probe the LB films of a bisphenolate zinc(II) complex $[Zn^{II}(L^{N2O2})H_2O]$ (**1**) and a bulkier trisphenolate gallium(III) complex $[Ga^{III}(L^{N_2O_3})]$ (**2**) (Figure 1) as mitigators for pit corrosion when physisorbed onto 99.0% aluminum substrates. The presence of hydrophobic *tert*-butyl groups installed to the phenolate groups along with hydrophilic alkoxy chains installed to the phenylenediamine bridge renders these species amphiphilic, enabling the formation of ordered molecular films. The presence of redox-inactive $3d^{10}$ ions like Zn^{II} or Ga^{III} confers added structural resistance to the organic framework limiting mobility of adventitious chlorides, and increases the energies of the ligand-based (LUMOs), thus precluding electron transfer through the film. The results follow.

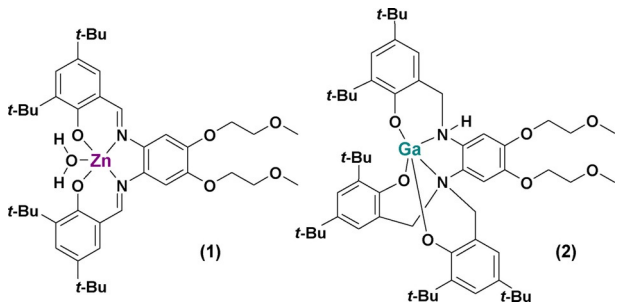

Figure 1. The metallosurfactants $[Zn^{II}(L^{N2O2})H_2O]$ (**1**) and $[Ga^{III}(L^{N2O3})]$ (**2**).

[a] *A. D. K. I. Weeraratne, C. C. Hewa-Rahinduwage, S. Gonawala, Prof. Dr. L. Luo, Prof. Dr. C. N. Verani*
Department of Chemistry, Wayne State University
5101 Cass Ave, Detroit, MI 48202 (USA)
E-mail: gk5120@wayne.edu
cnverani@wayne.edu
Homepage: http://chem.wayne.edu/veranigroup/

Supporting information and the ORCID identification number(s) for the author(s) of this article can be found under: https://doi.org/10.1002/chem.201903408.

The ligands $H_2L^{N_2O_2}$, $H_3L^{N_2O_3}$ and the Zn^{II} species **1** were synthesized as previously described.[17,18] The Ga^{III} species **2** was obtained by treating one equivalent of the ligand $H_3L^{N_2O_3}$ with one equivalent of $GaCl_3$ in the presence of three equivalents of $NaOCH_3$ in a $MeOH/CH_2Cl_2$ mixture under inert conditions (Figure S1, Supporting Information). The associated mass spectrum showed a peak at $m/z = 977.55$ attributed to $[Ga^{III}L^{N_2O_3} + H^+]^+$ in MeOH and elemental analysis is in excellent agreement with the calculated composition for **2**. The FTIR and UV/Vis spectroscopies confirm the amine character of the species (see Figures S2 and S3 and Tables S1 and S2, Supporting Information), as expected for complexes synthesized under anaerobic conditions.[18]

CV of **1** and **2** were performed in 1.0×10^{-3} mol L^{-1} CH_2Cl_2 solution using $TBAPF_6$ as a supporting electrolyte. Potentials were recorded versus the Fc^+/Fc couple. The CV of **1** was recorded previously[17] and displays well-behaved oxidation processes at 0.22 $V_{Fc/Fc+}$ ($\Delta E_p = 0.78$ V, $|I_{pa}/I_{pc}| = 0.9$) and at 0.56 $V_{Fc/Fc+}$ ($\Delta E_p = 0.16$ V, $|I_{pa}/I_{pc}| = 1.2$). Species **2** showed similar features at 0.43 and 0.77 $V_{Fc/Fc+}$ ($\Delta E_p = 0.10$ and 0.22 V, respectively, Figure 2). These processes are attributed to phenolate-to-phenoxyl radical conversion[19,20] with no metal-based reduction observed. The first oxidation is a quasi-reversible 1 e^- process, while the second is an irreversible 2 e^- process, as described in other gallium(III) species in similar environments.[22]

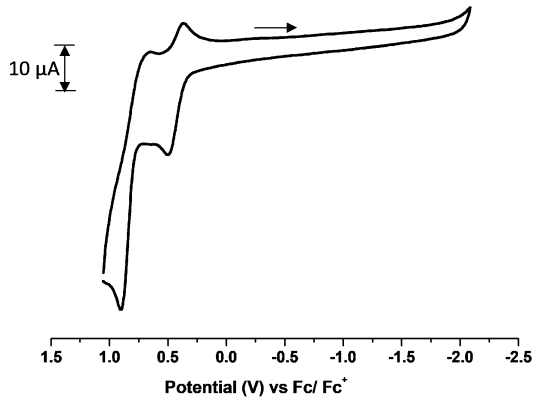

Figure 2. Cyclic voltammogram for $[Ga^{III}(L^{N_2O_3})]$ (**2**) (1 mM) in DCM. $TBAPF_6$, glassy carbon (WE), Pt wire (AE), Ag/AgCl (RE). Ferrocene is used as an internal standard. Scan rate :100 mV s^{-1}.

To mitigate corrosion, metallosurfactants must be deposited and physisorbed onto the metal substrate. Langmuir–Blodgett films were deposited using isothermal compression and the behavior of species **1** and **2** at the air/water interface was assessed by surface pressure (Π, mN m^{-1}) versus average area per molecule (A, $Å^2$ $molecule^{-1}$) plots and Brewster angle microscopy (BAM). Compression isotherms were performed in a minitrough with movable barriers triggering 2D activities at the air/water interface that lead to the formation of Langmuir–Pockels films. The assessment of mono- or multilayers, collapse pressures (π_c), and the area at the collapse of the monolayer (A_c) can be extrapolated. When the barriers are compressed, the tension (γ) of the amphiphile-containing air/water interface decreases as compared to that of the air/water interface only ($\gamma_0 = 72$ mN m^{-1} at 23 °C), following an increase in Π ($=\gamma_0-\gamma$). When compression is concomitant to BAM, polarized light passes throughout media with different refractive indexes at the air/water interface revealing agglomerates and domains, as well as film homogeneity in their absence. The behavior of **1** has been described[17] and shows an interaction area of 60 $Å^2$ $molecule^{-1}$ with collapse pressure at 45 mN m^{-1}. The isotherm and BAM for the Ga^{III}-containing **2** are shown in Figure 3. This species displays interaction in a vaporlike phase

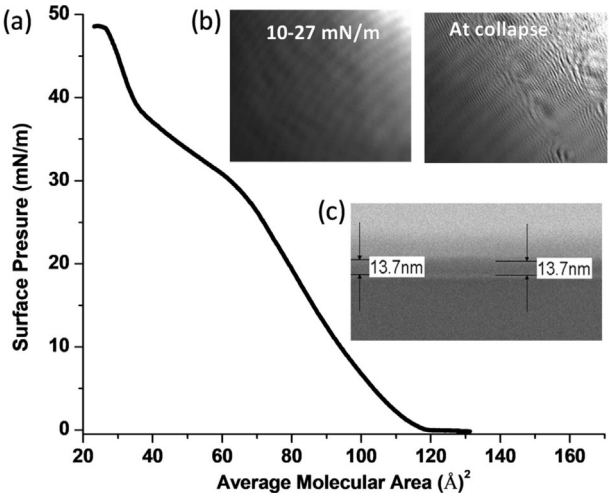

Figure 3. (a) Isothermal compression curve for **2**. (b) Selected BAM micrographs (c) SEM image of the cross section of 13 layers.

at ca. 117 $Å^2$ $molecule^{-1}$ (Figure 3 a). Between 10 and 27 mN m^{-1} a homogeneous liquid-expanded phase is observed, as supported by lack of BAM activity. Phase rearrangement was observed between 28 and 37 mN m^{-1}, likely leading to a condensed phase between 38 and 45 mN m^{-1}. Above 42 mN m^{-1} the formation of multiple ring-shaped events[21] associated with multilayer granules resulting from the ejection of matter from the compressed monolayer start to be noticeable and account for the thermodynamic instability and ultimate collapse of the film at ca. 48 mN m^{-1} (Figure 3 b). Collapse follows a Ries constant pressure mechanism.[18,22–25] These air/water Langmuir-Pockels films were later transferred onto air/solid interfaces at different surface pressures yielding Langmuir–Blodgett films.

The composition, topology, and defects of the LB films were investigated by IR reflection absorption spectroscopy (IRRAS). A total of 50 layers of LB-films were deposited keeping the transfer ratio close to unity and using a Y-type dipping method. Data was collected using *p*-polarized light at respective angles of incidence of 20 and 40° for **1** and **2**. While the results for **1** were previously discussed,[17] **2** displayed asymmetric and symmetric C–H stretching vibrations at ca. 2860–2960 cm^{-1}. The slight shift in the asymmetric C–H stretching vibrations in LB film compared to bulk correlates well with previous studies.[18,24] In the fingerprint region, bands around

1350–1610 cm^{-1} are assigned to aromatic C=C stretching vibrations and CH_n deformation bands. A new band at 1592 cm^{-1} and absent in the bulk IR spectrum was assigned to C=N stretching associated with amine-to-imine conversion at the air/water interface. This is a common occurrence for these systems.[18] Another feature in the IRRAS spectrum is that C–H stretching peaks are pointing upwards (positive) while other peaks are pointing downward (negative). This can be explained by the surface selection rules which states that positive bands are for vibrations with perpendicular transition dipole moments, and negative bands are for vibrations with parallel transition dipole moments. This inversion is due to the formation of anisotropic films with high molecular order (Figure S4, Supporting Information).[26–28] Static contact angle measurements were taken to evaluate the characteristic of the 99.0% aluminum substrates and infer the orientation of the molecules in the film. Species **1** and **2** showed respective contact angles of 92.55 and 90.97°, which when compared to the bare aluminum substrate at 86.47°, confirms enhancement of surface hydrophobicity. This indicates that the *tert*-butyl rich portions of both metallosurfactants point outwards. This observation is similar to other structurally related metal/phenolate systems.[17,18]

Pitting is particularly pronounced in Al| metal junctions[29] and in order to optimize electron passivation, films containing an increasing number of LB layers were probed by CV experiments with 1.0×10^{-3} M $K_3[Fe^{III}(CN)_6]$ in 0.1 M KCl aqueous solution at room temperature. The idea is to investigate how many layers are necessary to completely avoid electron transfer from an electrode to a good acceptor such as an Fe^{III} complex in a redox process given by $[Fe^{III}(CN)_6]^{3-} + 1\,e^- \rightarrow [Fe^{II}(CN)_6]^{4-}$. A standard electrochemical cell was used, in which LB films of **1** and **2** were deposited on Au plates acting as working electrodes with Ag/AgCl and Pt wire acting, respectively, as the reference and auxiliary electrodes. For Zn^{II}-containing **1**, optimal electron passivation was attained with a maximum residual current of 0.002 mA on films containing 11 layers deposited at 33 $mN\,m^{-1}$.[17] The ligands $H_2L^{N_2O_2}$ and $H_3L^{N_2O_3}$ showed larger residual currents at 0.025 and 0.024 mA, respectively (Figure S6, Supporting Information); therefore, in a tenfold increase. Monolayers of **2** were probed at three different surface pressures (20, 30, and 40 $mN\,m^{-1}$) and optimal electron passivation was observed at 40 $mN\,m^{-1}$. (Figure 4a). Because this surface pressure precedes the point in which ring-shaped events appear (42 $mN\,m^{-1}$) the formation of condensed monolayers is assumed. Therefore, this surface pressure was selected for additional depositions. Maximum passivation was attained with a residual current of 0.006 mA (Figure 4b). The results suggest that the use of metallated surfactants lead to enhanced electron passivation compared to their respective ligands. These results seem to confirm that redox-inactive $3d^{10}$ ions increase the energy of the ligand-based LUMOs precluding electron transfer through the film. Furthermore, surfactant **1** shows superior electron passivation, possibly due to packing and film thickness. To investigate this aspect, the thickness of the films for **1** and **2** was determined by SEM. Eleven layers of metallosurfactant **1** and thirteen layers of **2** were deposited on silicon

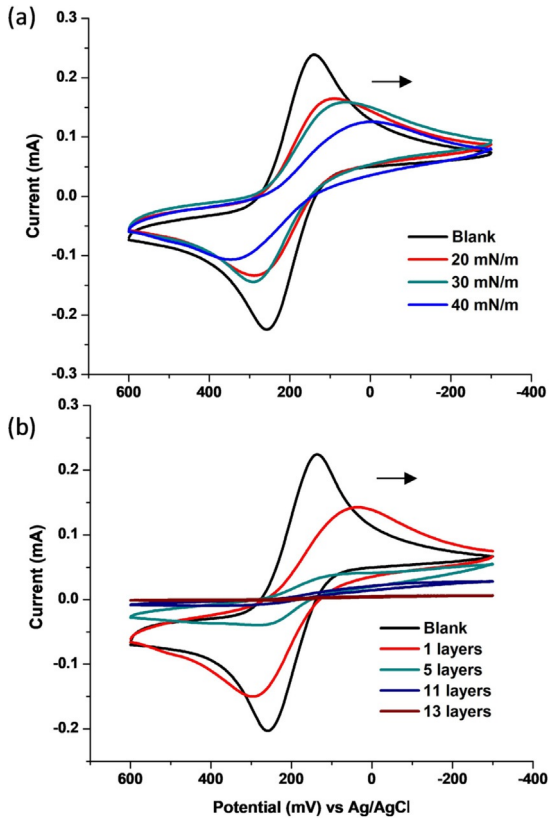

Figure 4. (a) CVs for the passivation of Au electrode with LB monolayers of **2** at different surface pressures, (b) CVs for passivation of Au electrode with different LB layers of **2**, at 40 $mN\,m^{-1}$. CVs were performed in 1.0×10^{-3} M $K_3[Fe^{III}(CN)_6]$ in 0.1 M KCl aqueous solution at room temperature and scan rate of 100 $mV\,s^{-1}$.

thermal oxide wafers and the thickness of the cross-section was measured. The average thickness for 11 layers of the Zn^{II}-containing **1** was 14.0 nm, whereas 13 layers of the Ga^{III}-containing **2** yielded 13.2 nm (Figure 3c and Figure S5, Supporting Information). The film of $[Zn^{II}(L^{N_2O_2})H_2O]$ (**1**) showed a larger thickness compared to that of $[Ga^{III}(L^{N_2O_3})]$ (**2**), suggesting that the bulky trisphenolate ligand tilts while forming the film. This observation is in good agreement with the results of a recent in situ spectroelectrochemical study on the orientation changes of a monolayer film of an Fe^{III}-containing metallosurfactant with the same ligand deposited on an Au electrode.[30] Metallosurfactant **1**, based on a bisphenolate ligand, seems to form a well-ordered film.

SEM images were recorded to evaluate the extent of pitting corrosion on aluminum substrates immersed in 3.5% NaCl solutions for different time periods. This environment simulates that found in seawater, and pitting was observed as conical or hemispherical shaped cavities with white gelatinous aluminum hydroxide at the rim of the pits. After being immersed in saline medium for five days, the unprotected bare aluminum substrate showed considerably more pithole defects compared to those aluminum substrates protected by the deposition of molecular LB films. However, substrates protected with films of the unmetallated ligands displayed more pitting than those substrates protected by Zn^{II}- and Ga^{III}-containing metallosurfac-

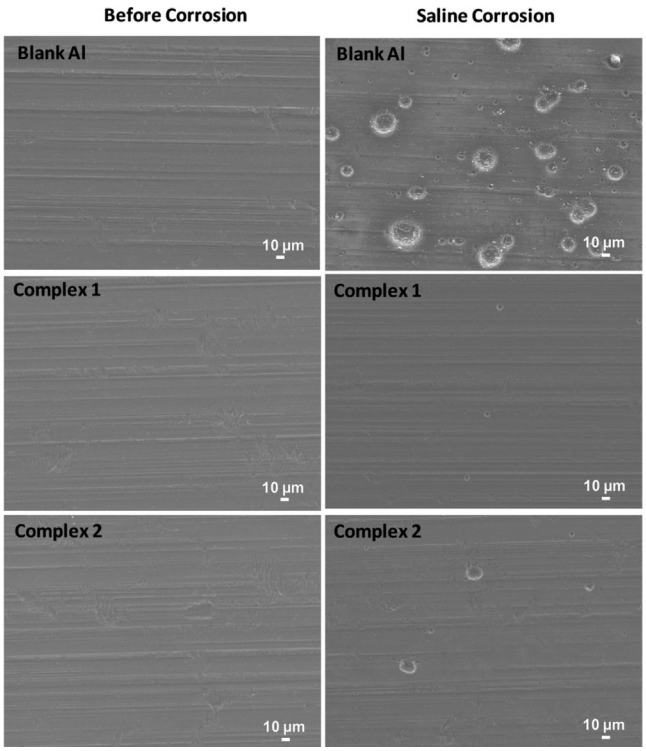

Figure 5. SEM images of Al substrates: blank, 11-layer LB film of **1** and 13-layer LB film of **2** after 10 days immersed in 3.5% NaCl solution.

tants. After 10 days of immersion the protected aluminum substrates showed dramatically less corrosion than the unprotected aluminum substrates (Figure 5 and Figure S7, Supporting Information).

To study the corrosion resistance properties of the LB films, potentiodynamic polarization experiments were performed by employing a three-electrode cell with the sample as the working electrode, Pt wire as the auxiliary electrode and Ag/AgCl as the reference electrode. By extrapolating the linear parts of the anodic and cathodic curves to their intersection, we can obtain the corrosion potential (E_{corr}) and the corrosion current (i_{corr}). Inhibition efficiency can be calculated from the measured i_{corr} values based on Equation (1):[31]

$$\%\ \text{Inhibition efficiency} = (i_{corr} - i'_{corr}/i_{corr}) \times 100 \qquad (1)$$

in which, i_{corr} and i'_{corr} are the corrosion current values of the bare aluminum and LB-film coated aluminum, respectively. Both samples and blank were immersed in 3.5% NaCl for 30 min at room temperature before potentiodynamic polarization studies. The corrosion potentials of (i) bare substrate, (ii) Ga^{III}-containing **2**, and (iii) Zn^{II}-containing **1** were −0.825, −0.789, and −0.764 V, respectively. In saline medium, corrosion current for bare aluminum substrate was 9.929 μA cm^{-2}. The $[Zn^{II}(L^{N_2O_2})H_2O]$ (**1**) surfactant displayed a corrosion current of 2.248 μA cm^{-2}, associated with the inhibition efficiency of 77%, while the $[Ga^{III}(L^{N_2O_3})]$ (**2**) surfactant exhibited corrosion current of 3.766 μA cm^{-2} with a inhibition efficiency of 62%. Increase in the corrosion potential and decrease in the corrosion current density of the substrates protected by the molecular films are evidence for the corrosion inhibition efficiency of **1** and **2**.[32] The Zn^{II}-containing species **1** showed higher inhibition efficiency compared to the Ga^{III}-containing **2** (Figure 6).

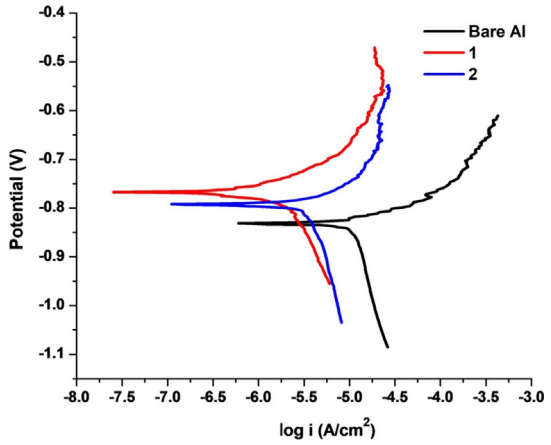

Figure 6. Potentiodynamic polarization curves after 30 min exposure to 3.5% NaCl. A scan rate of 10 mV s^{-1} was used for the experiment performed in 3.5% NaCl solution.

The corrosion resistance properties of metallosurfactants **1** and **2** were further investigated by electrochemical impedance spectroscopy (EIS). All data were collected at the open circuit potential in 3.5% NaCl. Figure 7a shows the Nyquist plots for the bare aluminum and the samples with different coatings (including **1**, **2**, $H_2L^{N_2O_2}$ and $H_3L^{N_2O_3}$). The EIS data were fitted to an equivalent circuit (Figure 7b) to obtain the charge-transfer resistance (R_{ct}, Table S3, Supporting Information). Both aluminum substrates coated with **1** and **2** show significantly larger R_{ct} than the bare, unprotected substrate (73 and 53 vs. 18 kΩ cm^{-2}, respectively). Because aluminum substrates coated with the ligands $H_2L^{N_2O_2}$ and $H_3L^{N_2O_3}$ exhibited similar R_{ct} as the blank, the increased R_{ct} values give evidence of the structural

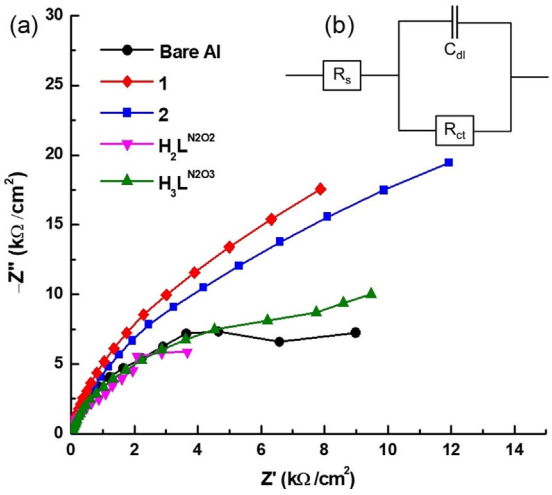

Figure 7. (a) Overlay of Nyquist plots for the blank aluminum and the aluminum substrates with different coatings. EIS experiments were performed in 3.5% NaCl solution. (b) Equivalent circuit used for modelling the EIS data.

role of redox-inactive metal ions such as zinc and gallium in metallosurfactants for molecular films and coatings.

In summary, we have evaluated the behavior of two metallosurfactants, $[Zn^{II}(L^{N_2O_2})H_2O]$ (**1**) and $[Ga^{III}(L^{N_2O_2})]$ (**2**), along with their metal-free and protonated ligands as precursors for molecular films capable of inhibiting pitting corrosion on aluminum surfaces. CV experiments indicate that 11–13 LB layers suffice to passivate electron transfer much more effectively than their respective ligands. SEM images, potentiodynamic polarization studies and impedance spectroscopy confirmed that both molecular LB films of **1** and **2** inhibit corrosive pitting, with the Zn^{II} species showing superior mitigation associated with an inhibition efficiency of 77%. This high inhibition is explained by structural and electronic contributions of the $3d^{10}$ metal ions, as well as by the thickness and order of the LB films. As such, the thicker and better ordered **1** passivates electron transfer more efficiently.

These results clearly evidence the value of molecular films based on nonredox metallosurfactants in the mitigation of pitting corrosion on aluminum surfaces. Ongoing studies involve enhancement of ligand hydrophobicity and use of covalent interactions between molecular film and the Al_2O_3 layer that covers the metal substrate.

Experimental Section

Materials and methods

Solvents and reagents were purchased from commercial sources and used without purification. ^{1}H NMR spectra were obtained using Varian 400 MHz instrument. A Bruker Tensor 27 FTIR spectrophotometer was used to obtain IR spectra of the bulk samples as KBr pellets. The window of measurement was between 4000 and 650 cm^{-1}. Elemental analysis was performed by Midwest Mictrolab in Indianapolis using an Exeter CE440 CHN analyzer. ESI-positive mass spectra were measured using a triple quadrupole Micromass Quattro LC instrument. UV/Vis spectra were measured in dichloromethane in the range of 200 to 1100 nm using a SHIMADZU UV-3600 spectrophotometer. Cyclic voltammograms were performed using a BAS 50 W potentiostat with a standard three electrode-cell consisting of a glassy-carbon working electrode, a Pt auxiliary electrode, and an Ag/AgCl reference electrode. $TBAPF_6$ was used as the supporting electrolyte and potentials were recorded versus the Fc^+/Fc couple.

Isothermal compression

Curves were measured using a KSV 2000 minitrough with Barnstead NANOpure water as the liquid subphase at a temperature of 23 °C. Impurities on the surface of the subphase were removed by vacuum suction. A 31 μL of 1.0 mg mL^{-1} chloroform solution of the metallosurfactant was introduced on the subphase and allowed to stand for 20 minutes before compression. Surface pressure vs. average molecular area isotherms were obtained at a compression rate of 10 mm min^{-1}. The Wilhelmy plate method was used to measure the surface pressure. Films were deposited onto a glass substrate at 40 $m_N m^{-1}$ and the transfer ratio was kept near unity. LB film characterization was done using IRRAS and UV/Vis spectrum of the film. The IRRAS spectrum was measured using a Bruker Tensor 27 infrared spectrometer with a Pike A 513/Q variable-angle accessory. UV–visible spectrum of the LB film was taken using a SHIMADZU UV-3600 spectrophotometer. The static contact angles of the films deposited on aluminum substrates were determined by KSV CAM 200 goniometer equipped with a CCD camera at room temperature.

Electron passivation studies

Performed using the BAS 50W potentiostat with three electrode-cells. LB films were deposited on Au electrodes and used as working electrodes. Cyclic voltammograms were performed for LB films deposited at different surface pressures and different numbers of layers.

Corrosion analysis

Performed by using 99.0% pure, 0.20 mm thick aluminum foil which was precleaned by ethanol, then with ultrapure water and air dried. Scanning electron micrograph images and thickness measurements were taken using a JSM-7600 FE scanning electron microscope. Potentiodynamic polarization studies and impedance spectroscopy was performed by using a CHI650E potentiostat.

Syntheses

The ligands $[H_2L^{N_2O_2}]$, $[H_3L^{N_2O_3}]$ and the metallosurfactant $[Zn^{II}(L^{N_2O_2})H_2O]$ (**1**) were obtained as described.[17,18]

The metallosurfactant $[Ga^{III}(L^{N_2O_3})]$ (**2**): This product was obtained by treatment of the ligand (0.301 g, 0.330 mmol in anhydrous methanol and dichloromethane (15 mL:5 mL)) with anhydrous $GaCl_3$ (0.058 g, 0.330 mmol) in presence of anhydrous $NaOCH_3$ (0.054 g, 0.990 mmol). The resulting solution was warmed at 50 °C for 30 min, and stirred for 2 h at ambient temperature. The solvent was completely removed, the crude product was dissolved in 20 mL dichloromethane, and filtered through Celite. Finally, the solvent was removed to allow precipitation of a yellow microcrystalline powder. Yield: 68%; elemental analysis calcd (%) for $[C_{57}H_{83}GaN_2O_7{\cdot}2H_2O]$: C 67.51, H 8.65, N 2.76; found: C 67.53, H 8.49, N 2.83; IR (KBR) $\tilde{\nu}$ = 3190 (ν_{N-H}), 2869–2964 (ν_{C-H}), 1607 ($\nu_{C=C,}$ aromatic), 1512 ($\nu_{C=C,}$ aromatic), 1269 ($\nu_{C\text{-}O\text{-}C}$), 1130 cm^{-1} ($\nu_{C\text{-}O\text{-}C}$); ^{1}H-NMR ($CDCl_3$, 400 MHZ): δ = 1.28 (s, 18 H^{tBu}), 1.62 (s, 18 H^{tBu}), 1.07 (s, 9 H^{tBu}), 1.48 (s, 9 H^{tBu}), 3.44 (s, 3 H^{OCH_3}), 3.52 (s, 3 H^{OCH_3}), 3.76 (t, 2 H^{OCH_2}), 3.85 (t, 2 H^{OCH_2}), 3.99 (s, 1 H^{CH_2}), 4.01 (s, 1 H^{CH_2}), 4.17 (m, 4 $H^{OCH_2,\ CH_2}$), 4.31 (t, 2 H^{OCH_2}), 4.52 (s, 2 H^{CH_2}), 6.41 (s, 1 H^{ph}), 6.79 (s, 2 H^{ph}), 6.90 (s, 1 H^{ph}), 6.98 (s, 2 H^{ph}), 7.04 (s, 1 H^{ph}), 7.17 ppm (s, 1 H^{ph}).

Acknowledgements

This work is funded by the National Science Foundation through grants NSF-CHE-1500201 and NSF-CHE1904584 to C.N.V., including partial support to A.D.K.I.W. L.L. thanks the Wayne State University for start-up funds, Ebbing Faculty Development Award, and the University Research Grant. A.D.K.I.W is a recipient of a Thomas C. Rumble Fellowship from the Graduate School at WSU.

Conflict of interest

The authors declare no conflict of interest.

Keywords: aluminum corrosion · aluminum pitting · gallium complexes · metallosurfactants · zinc complexes

[1] S. Das, *JOM* **2012**, *64*, 285 – 290.
[2] E. McCafferty, *Introduction to Corrosion Science*, Springer, Heidelberg, **2010**.
[3] A. Moschona, N. Plesu, G. Mezei, A. G. Thomas, K. D. Demadis, *Corros. Sci.* **2018**, *145*, 135 – 150.
[4] K. D. Demadis, C. Mantzaridis, R. G. Raptis, G. Mezei, *Inorg. Chem.* **2005**, *44*, 4469 – 4471.
[5] M. Frey, S. G. Harris, J. M. Holmes, D. A. Nation, S. Parsons, P. A. Tasker, R. E. Winpenny, *Chem. Eur. J.* **2000**, *6*, 1407 – 1415.
[6] J. M. Thorpe, R. L. Beddoes, D. Collison, C. D. Garner, M. Helliwell, J. M. Holmes, P. A. Tasker, *Angew. Chem. Int. Ed.* **1999**, *38*, 1119 – 1121; *Angew. Chem.* **1999**, *111*, 1191 – 1193.
[7] P. Natishan, W. O'Grady, *J. Electrochem. Soc.* **2014**, *161*, C421 – C432.
[8] M. A. Amin, S. S. A. El-Rehim, E. E. El-Sherbini, S. R. Mahmoud, M. N. Abbas, *Electrochim. Acta* **2009**, *54*, 4288 – 4296.
[9] E. McCafferty, *Corros. Sci.* **2003**, *45*, 1421 – 1438.
[10] L. Lin, C. Chao, D. Macdonald, *J. Electrochem. Soc.* **1981**, *128*, 1194 – 1198.
[11] D. D. Macdonald, *J. Electrochem. Soc.* **1992**, *139*, 3434 – 3449.
[12] E. McCafferty in *Surface Chemistry of Aqueous Corrosion Processes*, Springer, Heidelberg, **2015**, pp. 71 – 75.
[13] E. J. Thompson, T. W. Myers, L. A. Berben, *Angew. Chem. Int. Ed.* **2014**, *53*, 14132 – 14134; *Angew. Chem.* **2014**, *126*, 14356 – 14358.
[14] P. Natishan, E. McCafferty, *J. Electrochem. Soc.* **1989**, *136*, 53 – 58.
[15] W. G. Fahrenholtz, M. J. O'Keefe, H. Zhou, J. Grant, *J. Surf. Coat. Technol.* **2002**, *155*, 208 – 213.
[16] A. F. Carreira, A. M. Pereira, E. P. Vaz, A. M. Cabral, T. Ghidini, L. Pigliaru, T. Rohr, *J. Coat. Technol. Res.* **2017**, *14*, 879 – 892.
[17] S. Gonawala, V. R. Leopoldino, K. Kpogo, C. N. Verani, *Chem. Commun.* **2016**, *52*, 11155 – 11158.
[18] L. D. Wickramasinghe, M. M. Perera, L. Li, G. Mao, Z. Zhou, C. N. Verani, *Angew. Chem. Int. Ed.* **2013**, *52*, 13346 – 13350; *Angew. Chem.* **2013**, *125*, 13588 – 13592.
[19] M. Lanznaster, H. P. Hratchian, M. J. Heeg, L. M. Hryhorczuk, B. R. McGarvey, H. B. Schlegel, C. N. Verani, *Inorg. Chem.* **2006**, *45*, 955 – 957.
[20] L. Benisvy, E. Bill, A. J. Blake, D. Collison, E. S. Davies, C. D. Garner, C. I. Guindy, E. J. L. McInnes, G. McArdle, J. McMaster, C. Wilson, J. Wolowska, *Dalton Trans.* **2004**, 3647 – 3653.
[21] J. Galvan-Miyoshi, S. Ramos, J. Ruiz-Garcia, R. Castillo, *J. Chem. Phys.* **2001**, *115*, 8178 – 8184.
[22] H. E. Ries, Jr., *Nature* **1979**, *281*, 287.
[23] S. Kundu, A. Datta, S. Hazra, *Langmuir* **2005**, *21*, 5894 – 5900.
[24] L. D. Wickramasinghe, S. Mazumder, S. Gonawala, M. M. Perera, H. Baydoun, B. Thapa, L. Li, L. Xie, G. Mao, Z. Zhou, H. B. Schlegel, C. N. Verani, *Angew. Chem. Int. Ed.* **2014**, *53*, 14462 – 14467; *Angew. Chem.* **2014**, *126*, 14690 – 14695.
[25] A. D. K. I. Weeraratne, H. Baydoun, R. Shakya, J. Niklas, L. Xie, G. Mao, S. A. Stoian, O. G. Poluektov, C. N. Verani, *Dalton Trans.* **2018**, *47*, 14352 – 14361.
[26] G. Brezesinski, B. Dobner, C. Stefaniu, D. Vollhardt, *J. Phys. Chem. C* **2011**, *115*, 8206 – 8213.
[27] T. Hasegawa, J. Umemura, T. Takenaka, *J. Phys. Chem.* **1993**, *97*, 9009 – 9012.
[28] S. Joy, P. Pal, T. K. Mondal, G. B. Talapatra, S. Goswami, *Chem. Eur. J.* **2012**, *18*, 1761 – 1771.
[29] Z. Szklarska-Smialowska, *Corros. Sci.* **1999**, *41*, 1743 – 1767.
[30] I. Brand, J. Juhaniewicz-Debinska, L. Wickramasinghe, C. N. Verani, *Dalton Trans.* **2018**, *47*, 14218 – 14226.
[31] P. Manivel, S. Sathiyanarayanan, G. Venkatachari, *J. Appl. Polym. Sci.* **2008**, *110*, 2807 – 2814.
[32] X. Li, X. Nie, L. Wang, D. Northwood, *Surf. Coat. Technol.* **2005**, *200*, 1994 – 2000.

Manuscript received: July 25, 2019
Revised manuscript received: September 23, 2019
Accepted manuscript online: September 29, 2019
Version of record online: October 16, 2019